# Can a continuous mineral foam explain the stiffening of aged bone tissue?

## A micromechanical approach to mineral fusion in musculoskeletal tissues.

**R Penta[1], K Raum[2], Q Grimal[3], S Schrof[2], A Gerisch‡[1]**

[1] AG Numerik und Wissenschaftliches Rechnen, FB Mathematik, TU Darmstadt, Dolivostr. 15, 64293, Darmstadt, Germany

[2] Berlin-Brandenburg School for Regenerative Therapies, Charité Universitätsmedizin Berlin, Augustenburger Platz 1, 13353 Berlin, Germany

3 Sorbonne Universités, UPMC Univ Paris 06, CNRS, INSERM, Laboratoire d'Imagerie Biomédicale, F-75006, Paris, France

E-mail: `gerisch@mathematik.tu-darmstadt.de`

April 2016

**Abstract.** Recent experimental data revealed a stiffening of aged cortical bone tissue, which could not be explained by common multiscale elastic material models. We explain this data by incorporating the role of mineral fusion via a new hierarchical modeling approach exploiting the asymptotic (periodic) homogenization (AH) technique for three dimensional linear elastic composites. We quantify for the first time the stiffening that is obtained by considering a fused mineral structure in a softer matrix in comparison with a composite having non-fused cubic mineral inclusions.

We integrate the AH approach in the Eshelby-based hierarchical mineralized turkey leg tendon model [Tiburtius et al., Biomech Model Mechanobiol, 2014, DOI: 10.1007/s10237-013-0550-8], which can be considered as a base for musculoskeletal mineralized tissue modeling. We model the finest scale compartments, i.e. the extra-fibrillar space and the mineralized collagen fibril, by replacing the self-consistent scheme with our AH approach. This way, we perform a parametric analysis at increasing mineral volume fraction, by varying the amount of mineral that is fusing in the axial and transverse tissue directions in both compartments. Our effective stiffness results are in good agreement with those reported for aged human radius and support the argument that the axial stiffening in aged bone tissue is caused by the formation of a continuous mineral foam. Moreover, the proposed theoretical and computational approach supports the design of biomimetic materials which require an overall composite stiffening without increasing the amount of the reinforcing material.

*Keywords*: Multiscale composites, Asymptotic homogenization, Bioinspired materials, Aged bone stiffening, Mineral fusing

‡ corresponding author

## 1. Introduction

Musculoskeletal mineralized tissues (MMTs), such as tendons and bones, can be regarded as *multiscale composite materials* [1, 2, 3, 4] as their basic constituents interplay on several hierarchical levels of organization [5, 6]. The main constituents of MMTs are collagen, mineral crystals (in the form of hydroxyapatite), and water. The multiscale nature of MMTs implies that information concerning solely the relative amount of the individual constituents is not sufficient to fully determine their mechanical or other properties. It is indeed crucial to capture the details of the mutual interplay among the various basic constituents and the way they interact to arrange across several (up to seven for human bone [5]) spatial scales to form the tissue scale MMT structure. Although the composition and multiscale arrangement of these constituents strongly depend on the specific tissue type, it is possible to identify the mineralized collagen fibril (MCF) as a common fine scale structural motif in all mineralized tissues.

The MCF consists of self-assembled collagen molecules that align parallel in staggered arrays, see Fig. 1 a). Hydroxyapatite crystals nucleate and grow within this organic matrix, see Fig. 1 b), both in the intrafibrillar space, reinforcing the collagen fibrils, and in the extrafibrillar space (ES), which primarily consists of mineral and water, [5].

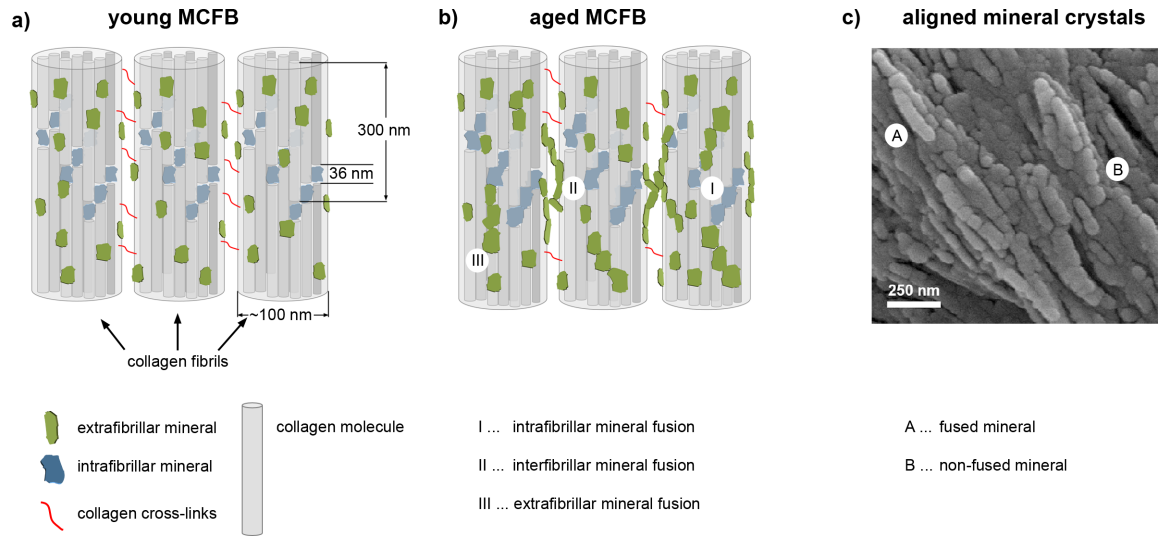


**Figure 1:** a) Model of a young mineralized fibril bundle (MCFB). Collagen molecules are stacked in a fibril. Mineral crystals nucleate first within the gap regions (blue) and then also in the extrafibrillar space (green). Adjacent fibrils are connected by collagen cross-links. b) Tissue aging leads to crystal growth and nucleation of more crystals. The latter occurs predominantly in the extrafibrillar space. Adjacent crystals can fuse (I-III). The fusion of crystals between adjacent fibrils (II) establish a rigid fusion, eventually replacing the function of the more flexible collagen cross-links. c) The development of aligned and partially fused crystal chains can also be seen in scanning electron micrographs of deproteinized bone; image reproduced from [7] with permission.

The mechanical properties of the mineral and collagen phase play a crucial role in the setup of any macroscopic MMT model. More specifically, changes in the collagen

properties have a stronger influence on macroscopic toughness and strength (see, e.g., [8]), whereas the crystal organization at the nanometer level can substantially affect the macroscopic tissue behavior in terms of elastic stiffness. Relevant examples of mineral crystal modeling may incorporate structural information such as crystal particles size and shape, spacing in directions along and transverse to the crystal c-axis, and crystal orientation. The approach reported by Currey in [9] represents a first, pioneering attempt to account for the observed rise of the bone stiffness with increasing mineral content, which appears to be steeper than the rise that would be observed in a composite with embedded fibers. The author explained this behavior by means of the analytical model [10] (which provides an estimate of the Young's modulus of the MCF assuming a cylindrical crystal shape) considering an end-to-end fusion of the crystals at increasing mineral volume fraction. In [11], the basic crystal-collagen compound is considered as a platelet-reinforced composite (rather than a fiber-reinforced one) and modeled via the approach [12], where the crystals geometry is specified in terms of thickness, width and length. In [13], the mineral crystals are modeled as staggered arrays, unlike previous works where parallel arrays are considered. The latter model captures the increase of both the stiffness and the fracture stress at increasing mineralization as well as the role of the shear forces in the collagen matrix. Essential limitations of the above mentioned models are that a) they essentially provide an estimation of the Young's modulus (in the direction of the crystal axis) only and b) they are based on ad-hoc assumptions on the type of interaction between the collagen and the mineral or on the strain or stress fields.

Mean field techniques based on the analytical results introduced by Eshelby [14] are widely exploited in the literature, as they can predict all terms of the stiffness tensor semi-analytically, see, e.g., the MCF models developed in [15, 16, 17, 18, 19, 20, 21]. Eshelby-based models are formulated assuming ellipsoidal material inclusions, such that the geometry of embedded inclusions (such as the mineral crystals in the collagen matrix) is specified by their representative ellipsoid aspect ratios. Eshelby-based methods are also well suited to derive approximations of the elastic stiffness of hierarchical composites, such as MMTs, as the various Eshelby-based techniques can be applied in cascade across a wide range of spatial scales. Hellmich and co-workers have repeatedly used the concept of mineralized collagen fibrils embedded in a hydroxyapatite foam (with water and non-collagenous organic material in the inter-crystalline space), see, for instance, [15, 16, 21]. This compound (sometimes referred to as ultrastructure) is modeled with a mean field approach, based on Mori-Tanaka and self-consistent methods, that accounts for strong interactions between individual mineral particles in the mineral foam and between the fibrils and the mineral foam. However this approach assumes a random microstructure and as such does not allow to explicitly model a specific microstructural pattern [22]. In other words, for given phase volume fractions, mean field approaches do not distinguish between a fused end-to-end network of mineral crystals and a dense cloud of small (not connected) mineral crystals. In [23] we developed a multiscale Eshelby-based model for the hierarchical structure of the mineralized turkey

leg tendon (MTLT). We exploited a sequence of nested models to compute the apparent stiffness of MTLT on the basis of (a) The MCF and ES compartments, represented as collagen-mineral and mineral-water composites, respectively (b) the mineralized collagen fibril bundle (MCFB), modeled as composite consisting of an ES and an MCF phase, and (d) the MTLT, comprising the MCFB and the (micro) pores phases. The latter hierarchical model was experimentally validated by means of site-matched scanning acoustic microscopy (SAM) and synchrotron radiation microcomputed tomography (SR$\mu$CT) data (Fig. 2). In these studies, the ultrasound frequency and lateral confocal beam diameter (i.e. 50 MHz to 200 MHz and 25 $\mu$m to 8 $\mu$m, respectively) used for mapping the acoustic impedance as well as the voxel size and the spatial resolution for the tomographic assessment of the mineral volume fraction were carefully adjusted such that i) the interaction volumes for both modalities were comparable and ii) the compound tissue properties were measured. The quantitative influence of key parameters on the elastic stiffness tensor, such as the mineral volume fraction and the microporosity, was identified. Since the model accounts for unidirectionally aligned MCFs, and it is based on the characteristic MMT building blocks, the predictions of the transverse and axial elastic stiffness components can be viewed as upper and lower bounds for more generic bone tissues. In fact, a site-matched analysis of mineral volume fraction and elastic stiffness data from various bone tissues showed that the majority of the experimental data fell within these bounds, except for very old cortical bone, which exhibited stiffness values significantly above the predicted upper limit, see Fig. 2.

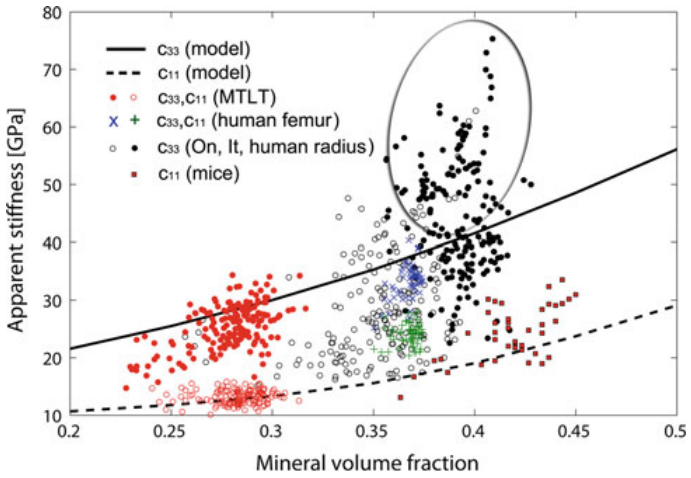


**Figure 2:** Predicted and measured elastic stiffness coefficients $\mathbf{C}_{11}$ (transverse) and $\mathbf{C}_{33}$ (axial) with respect to the mineral volume fraction. The experimental data have been obtained from various tissues and specimen, i.e. mineralized turkey leg tendon (MTLT) [23], human femur [24], human radius [25] and mice [26]. The lines show the upper and lower stiffness bounds predicted by the MTLT model proposed in [23]. The encircled data are predominantly from interstitial tissue regions and are clearly outside the range predicted by the MTLT model (reprinted from Tiburtius et al. [23] with permission).

These findings support the hypothesis that there exists a further mechanism (other than the increase of the mineral volume fraction only) driving MMTs stiffening, such as a tissue age dependent fusion of mineral crystals. This process arises as a consequence

of mineral growth and extrafibrillar mineral deposition, leading to the constitution of a continuous mineral foam. In this contribution we setup an innovative multiscale framework for MMTs that incorporates such a mechanism.

Clear experimental evidence of such a continuous mineral crystal structure with strong bounds between mineral particles was recently shown in [27] for mature bone. Compression tests were performed to show that the mineral phase, after removing the organic phase, still appears as a self-supporting network. In [28] the authors studied the architecture and microstructure of the mineral phase in deproteinized bone. Using electron microscopy, they demonstrated that the mineral phase in bone forms continuous, self-supporting fiber-like structures. These polycrystalline fibers feature a periodic spacing of crystallites along their long axis, which is consistent with the periodic bending pattern of the gap region in collagen fibrils. These observations support the hypothesis of an initial hydroxyapatite nucleation in the gap space within the MCF. The authors also observed the presence of hydroxyapatite bridges between the fibrils with the same spacing as the intrafibrillar crystal aggregation. These experimental observations on the mineral organization in bone suggest that the mechanical properties of mature bone are not only determined by the relative amount of crystals, but also by the interconnections between mineral crystallites. Although the nature of interconnecting bonds between mineral particles is not yet fully understood, recent findings [29] confirmed the presence of citrate bridges between mineral platelets that could be responsible for the formation of a continuous, self-supporting mineral structure. In [30], the authors observed stiffening of elderly women bone by means of nanoindentation. Moreover, they observed that both young and old bone softened towards the same stiffness value when increasing the nanoindentation depth, i.e. increasing the amount of broken mineral interconnections. A sketch of the mineral fusing phenomenon occurring at the mineralized collagen fibril bundle (MCFB) level is depicted in Fig. 1.

The aim of this work is the setup of a novel modeling framework broadly applicable to MMTs and capable to account for fused mineral structures both in the MCF and in the ES. We exploit our recent advances concerning the application of the asymptotic (periodic) homogenization technique for three dimensional composites [31] to capture the effective stiffness due to a fused skeleton embedded in a softer matrix. The fine scale geometry is identified with a periodic cell that comprises a softer phase (representing the collagen in MCF or the nanopores in ES) and a cross-shaped structure (representing the mineral phase) that extends up to the boundaries of periodic cell. This approach is then integrated in the sequence of nested models exploited in [23] by replacing the Eshelby based model in the ES and/or the MCF to quantify the stiffening effect due to both intra and extra fibrillar mineral fusing occurring to a different extent in the transverse and axial directions.

Our work is structured as follows:

- In Section 2, we summarize the asymptotic homogenization (AH) approach to compute the effective elasticity tensor for linear elastic composite materials with discontinuous material properties. This approach represents a suitable

approximation of the interplay between the different MMTs constituents. We perform an *in silico* experiment to quantify the axial and transverse stiffening that is obtained for a composite with a cross-shaped fused structure when compared to a composite having cubic inclusions occupying the same volume fraction.

- In Section 3, we setup hybrid models based on the MTLT model [23] by replacing the self-consistent scheme, exploited there to model the MCF and the ES, with our AH approach. In Section 3.1, we summarize the features of the multiscale model provided in [23], which serves as a starting point for our analysis. In Section 3.2, we show an example of how this model can be modified via AH with cuboid inclusions for the MCF. We validate this new hybrid model against the MTLT experimental results reported in [23], thus strengthening the reliability of our technique. In Section 3.3, we describe a novel hybrid model with AH for a fused mineral structure in the ES and perform a parametric analysis by varying the amount of mineral that is fusing in the axial and transverse directions (including the limit case of uniaxial fusing). In Section 3.4, we assume uniaxial fusing in the ES and apply such a parametric analysis to the case where AH is employed also for a fused mineral structure in the MCF. The axial stiffness results of Sections 3.3 and 3.4 are compared with the axial stiffness data measured for aged human radius, [25].
- In Section 4, we highlight the major novelties and discuss the results.
- In Section 5, we conclude the paper presenting future directions and challenges.

## 2. Mathematical and computational methodology

In [31, 32] the authors exploit the potential of the asymptotic homogenization technique (e.g., [33, 34, 35, 36, 37, 38, 39]) for composites with discontinuous materials properties, from a computational and theoretical viewpoint, respectively. They account for the coupling between a host (*matrix*) phase and another (or multiple) distinct linear elastic subphase via continuity of stresses and displacements at each matrix-subphase interface. Then they enforce a sharp length scale separation between a *fine scale* $d$, where details of the local structure are clearly identified and a *coarse scale* $L$ characterizing the whole composite, such that

$$\epsilon = \frac{d}{L} \ll 1, \text{ and } \boldsymbol{y} = \frac{\boldsymbol{x}}{\epsilon}, \tag{1}$$

where $\boldsymbol{x}$ and $\boldsymbol{y}$ represent the independent coarse and fine scale spatial variables, respectively. The classical asymptotic homogenization steps are then exploited, namely: (a) representation of the elastic displacement and individual constituent elastic properties as independent functions of $\boldsymbol{x}$ and $\boldsymbol{y}$ in both the matrix and the subphase(s); (b) series expansions of the solution in terms of the asymptotic parameter $\epsilon$; (c) fine scale periodicity; (d) upscaling to determine the coarse scale equations for the zero-th order component of the elastic displacement. This way, a system of elastic-type partial differential equations is obtained on the coarse scale $\boldsymbol{x}$, where the arising fourth rank

tensor $\tilde{\mathbb{C}}$, which is indeed the effective elasticity tensor for the composite (see [32]), reads:

$$\tilde{\mathbb{C}} = \left\langle \mathbb{C}^A + \mathbb{C}^A\mathbb{M}^A \right\rangle_A + \left\langle \mathbb{C}^B + \mathbb{C}^B\mathbb{M}^B \right\rangle_B , \tag{2}$$

where the integral average operators are defined as

$$\langle \bullet \rangle_A = \frac{1}{|\Omega|}\int_{\Omega_A} \bullet \ \mathrm{d}\boldsymbol{y}; \quad \langle \bullet \rangle_B = \frac{1}{|\Omega|}\int_{\Omega_B} \bullet \ \mathrm{d}\boldsymbol{y}. \tag{3}$$

Here, $\mathbb{C}^A$ and $\mathbb{C}^B$ represent the individual elasticity tensors for the matrix and the subphase, and $\Omega_A$ and $\Omega_B$ their corresponding portion of the periodic cell $\Omega$ (with associated total volume $|\Omega|$ and subphases volumes $|\Omega_A|$ and $|\Omega_B|$ ). The auxiliary fourth rank tensors $\mathbb{M}^A$, $\mathbb{M}^B$ are defined, componentwise, as

$$M^A_{pqkl} = \xi^{kl}_{pq}(\chi^A) = \frac{1}{2}\left(\frac{\partial \chi^A_{pkl}}{\partial y_q} + \frac{\partial \chi^A_{qkl}}{\partial y_p}\right), \tag{4}$$

$$M^B_{pqkl} = \xi^{kl}_{pq}(\chi^B) = \frac{1}{2}\left(\frac{\partial \chi^B_{pkl}}{\partial y_q} + \frac{\partial \chi^B_{qkl}}{\partial y_p}\right). \tag{5}$$

The third rank tensor $\chi$ (with restrictions $\chi^A$ and $\chi^B$ over $\Omega_A$ and $\Omega_B$, respectively) is the solution of the following periodic cell problems in $\Omega$:

$$\frac{\partial}{\partial y_j}\left(C^A_{ijpq}\xi^{kl}_{pq}(\chi^A)\right) = -\frac{\partial C^A_{ijkl}}{\partial y_j} \text{ in } \Omega_A, \tag{6}$$

$$\frac{\partial}{\partial y_j}\left(C^B_{ijpq}\xi^{kl}_{pq}(\chi^B)\right) = -\frac{\partial C^B_{ijkl}}{\partial y_j} \text{ in } \Omega_B, \tag{7}$$

$$C^A_{ijpq}\xi^{kl}_{pq}(\chi^A)n^B_j - C^B_{ijpq}\xi^{kl}_{pq}(\chi^B)n^B_j = (C^B - C^A)_{ijkl}n^B_j \text{ on } \Gamma, \tag{8}$$

$$\chi^A_{ikl} = \chi^B_{ikl} \text{ on } \Gamma, \tag{9}$$

where $n^B_j$ is the $j$-th component of the unit vector normal to the matrix-subphase interface $\Gamma = \partial\Omega_A \cap \partial\Omega_B$ and pointing into the subphase $\Omega_B$. In (6-9), summation over repeated indices $p, q, j$ is understood and the problem (6-9) is closed by periodic conditions on $\partial\Omega\backslash\Gamma$. Further conditions are to be imposed to ensure solution uniqueness, e.g.

$$\left\langle \chi^A_{ikl} \right\rangle_A = \left\langle \chi^B_{ikl} \right\rangle_B = 0 \quad i,k,l = 1,2,3. \tag{10}$$

The system (6-9) can be rewritten as six elastic-type boundary value problems equipped with interface loads proportional to the difference in the elastic constants across $\Gamma$, as shown in [31]. These interface loads play a crucial role in determining the solution of the cell problems and represent the only driving force whenever the two (or multiple) elastic phases are uniform, as the volume forces in (6, 7) vanish in that case.

Numerically we obtain the effective elasticity tensor $\tilde{\mathbb{C}}$ by firstly solving the elastic-type cell problems (6-9) to obtain the fourth rank tensors $\mathbb{M}^A$ and $\mathbb{M}^B$ given by (4,5) and secondly computing the effective elasticity tensor $\tilde{\mathbb{C}}$ via (2). We carry out the required 3D simulations using the scheme adopted in [31] employing the finite element software COMSOL Multiphysics.

Next we follow the AH approach for a cross-shaped structure, see Fig. 3, which represents, in a periodic setting, a fused skeleton embedded in a matrix phase.

### *2.1. Elastic stiffening for a cross-shaped structure*

We assume that the embedded phase $\Omega_B$ is stiffer than the matrix $\Omega_A$ and we aim at pointing out the stiffening that is arising as a result of merely fusing the geometry of the embedded subphase. To this end, we compare the effective stiffness that is obtained for a composite material made of cubic inclusions (as reported in [32]) to that obtained for a structure which is equally fusing along the three orthogonal directions (where we identify $\boldsymbol{e}_3$ and $\{\boldsymbol{e}_1, \boldsymbol{e}_2\}$ with the axial and transverse directions, respectively), as represented by the periodic cell depicted in Fig. 3. Since we focus on a geometrically

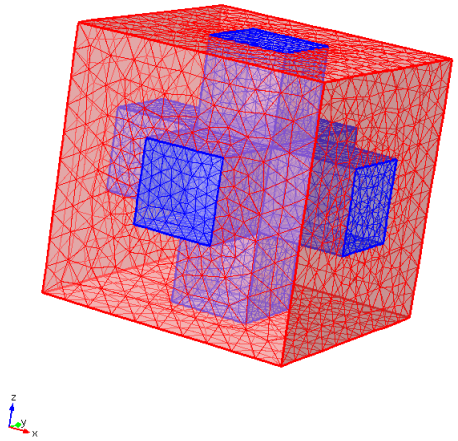

**Figure 3:** A cross-shaped periodic cell representing a structure equally fusing along the three orthogonal directions. The embedded stiff phase $\Omega_B$ and the softer matrix phase $\Omega_A$ are depicted in blue and red, respectively.

induced effect, we consider the simplest possible case for the material properties, i.e. the matrix $\Omega_A$ and the subphase $\Omega_B$ are isotropic and uniform elastic media, characterized by the Young's moduli and Poisson's ratios $E_A$, $E_B$ and $\nu_A$, $\nu_B$, respectively. We exploit the same values as in [31], thus referring to the values reported in [23] for the collagen matrix, $\Omega_A$, and the (hydroxyapatite) mineral phase, $\Omega_B$, in the bone, that is

$$E_A = 5\,[\text{GPa}];\ \nu_A = 0.3;\ E_B = 110\,[\text{GPa}];\ \nu_B = 0.28. \tag{11}$$

A cubic inclusion and the considered cross-shaped geometry are characterized by three orthogonal planes of symmetry and are invariant with respect to permutation of the three orthogonal axis, see, e.g., [40], hence we can represent the elasticity tensor (in the *Voigt* notation, see, e.g., [41]) in a cubic symmetric form (see, e.g., [42]) via the

following $6 \times 6$ symmetric matrix

$$\tilde{\mathbb{C}} = \begin{bmatrix} \tilde{C} & \tilde{C}_{12} & \tilde{C}_{12} & 0 & 0 & 0 \\ \tilde{C}_{12} & \tilde{C} & \tilde{C}_{12} & 0 & 0 & 0 \\ \tilde{C}_{12} & \tilde{C}_{12} & \tilde{C} & 0 & 0 & 0 \\ 0 & 0 & 0 & \tilde{C}_{44} & 0 & 0 \\ 0 & 0 & 0 & 0 & \tilde{C}_{44} & 0 \\ 0 & 0 & 0 & 0 & 0 & \tilde{C}_{44} \end{bmatrix}. \tag{12}$$

Hence, the elasticity tensor is fully specified by three independent parameters. The axial ($\tilde{C}_{33}$) and transverse ($\tilde{C}_{11} = \tilde{C}_{22}$) stiffness components are represented by the single parameter $\tilde{C}$. We perform a parametric analysis varying the mineral volume fraction $\phi_m = \dfrac{|\Omega_B|}{|\Omega|}$ in the range $0 < \phi_m < 0.5$, thus accounting for an upper limit which is consistent with the mineralized tissues scenario (see, e.g., [43]). The resulting $\tilde{C}$ values are plotted against the subphase (mineral) volume fraction in Fig. 4.

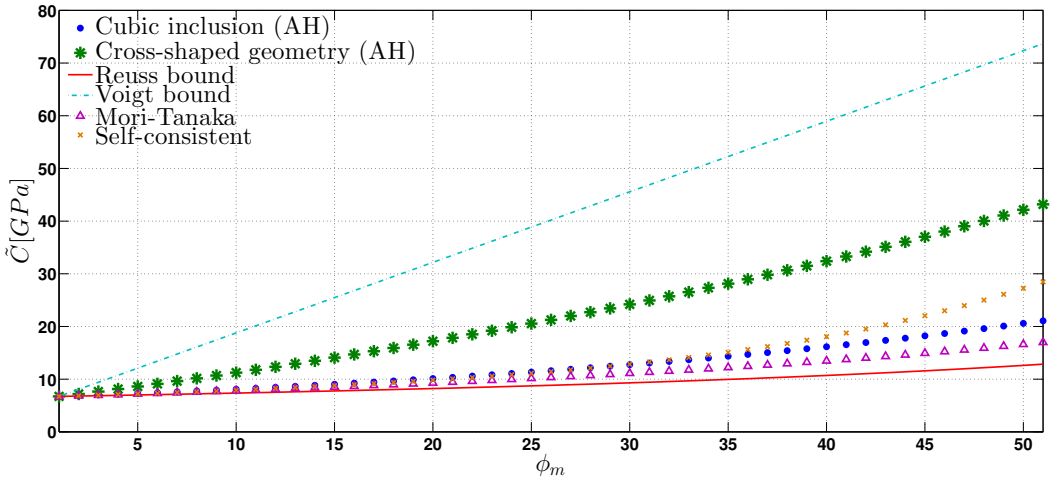


**Figure 4:** The effective stiffness $\tilde{C}$ versus mineral volume fraction for cubic inclusion, cross shaped structure, Reuss lower bound, Voigt upper bound, Mori-Tanaka method, and self-consistent scheme.

We also plot the well-known upper (Voigt [44]) and lower (Reuss [45]) bounds (that apply to every diagonal component of the effective elasticity tensor, cf. [32]), together with the self-consistent [46] and Mori-Tanaka [47] results using spherical inclusions. Our results quantify, for the first time, the geometrically induced stiffening due to fusing of an elastic three dimensional subphase embedded in a softer matrix, in the context of our asymptotic homogenization scheme. According to the results shown in Fig. 4, we report the following observations.

(a) The stiffness $\tilde{C}$ characterizing the fused structure is substantially greater (over 100% for $\phi_m$ approaching 50%) than the one obtained for a cubic inclusion at fixed volume fraction.

(b) We performed a comparison between the asymptotic homogenization scheme and Eshelby based [14] techniques, such as the Mori-Tanaka and self-consistent schemes. Since we can consider ellipsoidal inclusions only in the latter context, we considered spherical inclusions because the geometries exploited for our asymptotic homogenization analysis are invariant for permutation of the three orthogonal axis. The two approaches are comparable for non-fused inclusion phases only, whereas the remarkable stiffening obtained for a fused structure can only be captured via our asymptotic homogenization scheme, which allows for more flexibility in retaining the full details of the fine structure (see also the computational tests reported in [31]).

Next, we integrate the approach described in this section to model the MCF and ES compartments in unidirectionally aligned mineralized collagen fibril bundles. We also consider more flexible cross-shaped structures, such that the relative amount of fusion in the transverse and axial directions can be modified. This way we can construct a novel multiscale model which can be used as an approximation to capture the observed stiffening effect in old bone (see Fig. 2) and relate it to the formation of a continuous mineral foam (see Figs. 1 b) and 1 c)), as reported in [27] for mature bone.

## 3. MMTs with fusing minerals: multiscale model and results

Our aim is to setup a new hybrid multiscale model for musculoskeletal mineralized tissues to capture the stiffening effect caused by mineral fusing in the (human) bone. To this end, we start from the mineralized turkey leg tendon hierarchical model developed in [23], see also Fig. 5, and integrate the methodology of Section 2 in a way which allows to account for different relative amounts of mineral fusing in the axial and transverse directions. Table 1 gives an overview of the models considered in this section. Before describing the hybrid models, we first summarize the main features of the model [23] in the following subsection.

| Hierarchical model | MCF | ES |
|---|---|---|
| (a) Eshelby-based model, cf. [23] | SC | SC |
| (b) Hybrid model, cf. Section 3.2 | AH (cuboid inclusion) | SC |
| (c) Hybrid model, cf. Section 3.3 | SC | AH (fusing) |
| (d) Hybrid model, cf. Section 3.4 | AH (fusing) | AH (uniaxial fusing) |

**Table 1:** The MCF and ES modeling options presented in this paper involve combination of the asymptotic homogenization (AH) and self-consistent (SC) schemes. The elastic stiffness components of MCFB and MTLT are always computed via the Mori-Tanaka scheme.

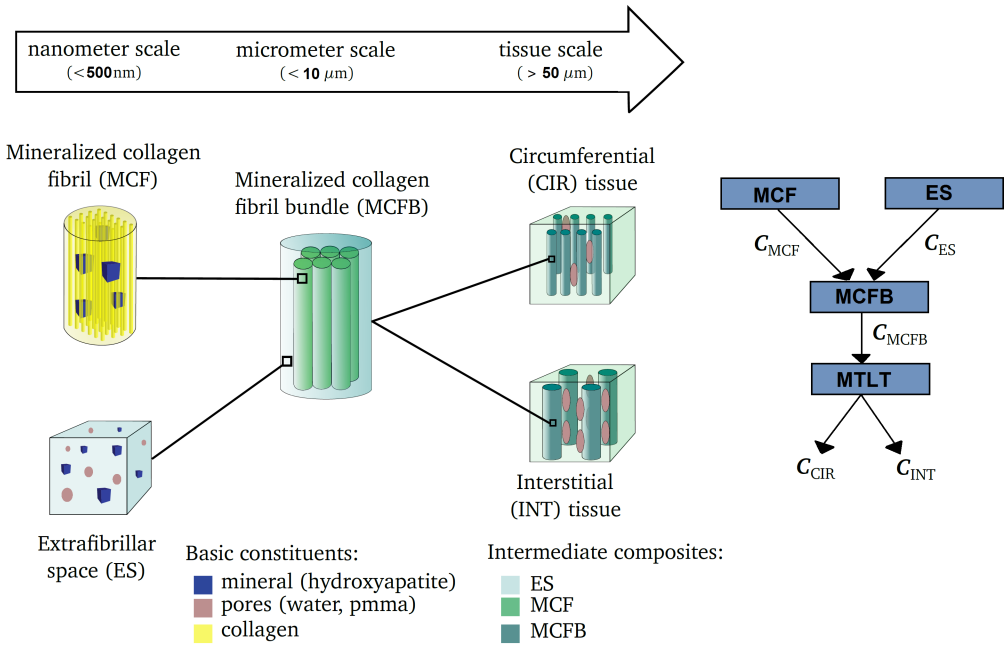


**Figure 5:** Model hierarchy of MTLT tissues (adapted with permission from [23], Fig. 3, page 1009) and a schematic of the nested sequence of models to compute the effective stiffness. The spatial scale separation and hierarchical level representation is also highlighted in [21] and references therein. The various modeling options are summarized in Table 1.

### *3.1. An Eshelby-based multiscale model of the MTLT*

In [23] the authors setup and validate a multiscale model for the MTLT characterized by the following main features:

- *Hierarchical structure.* The MTLT is a particular MMT, which is organized across several hierarchical levels spanning different spatial scales, from $\approx 1\,\text{nm}$ to $1-50\,\mu\text{m}$, see Fig. 5. The nanoscale level comprises unidirectionally aligned mineralized collagen fibrils (forming the MCF), composed of a collagen and a mineral phase, and the extrafibrillar space (ES), composed of water (filling "nanopores") and a mineral phase. At the next hierarchical level, multiple MCFs embedded in the ES form the mineralized collagen fibril bundle (MCFB), composed of an MCF and an ES phase. The last hierarchical level ($\approx 50\,\mu\text{m}$) under consideration is the MTLT tissue itself, which is composed of an MCFB phase and a water phase (filling "micropores"). Both water phases are replaced with polymethylmethacrylate (pmma) for the sake of consistency with the experimental data reported in [23], where the samples where embedded in pmma. This choice is also convenient as it allows to carry out the modeling analysis solely in the simplified framework of (linear) elasticity, rather than accounting for multiscale modeling of poroelastic materials.
- *Elastic properties of the basic constituents.* The basic tissue constituents, that is mineral, pores (pmma), and collagen, were modeled as isotropic elastic materials. The corresponding elastic parameters, as given in [23], are used in all computations reported in this work. Furthermore, the defining elastic moduli for mineral and

collagen are also given in Eq. (11).

- *Eshelby-based elastic modeling.* The hierarchical structure of the MTLT is modeled via an Eshelby-based approach [14], which provides the semi-analytical solution for the strain inside an ellipsoidal inclusion in an infinite medium subject to uniform strain conditions at infinity. Such a solution is exploited to construct several approximations by proper superpositions of the Eshelby solutions to compute the effective elasticity tensor of composite materials, depending on (a) individual constituent elastic properties, (b) ellipsoidal inclusions aspect ratios, (c) individual phase volume fractions. In [23], the ES and MCF are modeled via the self-consistent scheme. They are both assumed to be composed of two distinct phases, namely pmma-mineral and collagen-mineral, respectively. Individual phases are represented as ellipsoidal inclusions. The inclusions are then embedded in a homogeneous material whose stiffness is the one of the composite itself, leading to a nonlinear system of equations to determine the elastic stiffness. This procedure accounts for the interaction among inclusions and is particularly suited when dealing with non-diluted systems, as remarked in [16]. The MCFB is modeled via a more diluted Eshelby-based technique, namely the Mori-Tanaka scheme. In this case, the effective stiffness is computed considering the ES as a matrix and the MCFs as the embedded ellipsoidal inclusions. The matrix phase is clearly identified and it also acts as the homogeneous material where the inclusions are embedded. Moreover, the superposition of Eshelby-based solutions leads to a straightforward evaluation of the effective elasticity tensor. In the Mori-Tanaka scheme, the interactions between the inclusions and the matrix are not considered explicitly, although the inclusions "feel" the matrix through the constant strain at infinity (which is set to the average strain in the matrix).
- *Experimental validation.* The results obtained via the above described model have been validated against experimental data by means of acoustic impedance values corresponding to axial and transverse stiffness components. The relative root mean square error between the model and the experimental data is of the order of 6-8 %.
- *The MTLT model as an upper and lower bound for MMTs.* The MTLT model is based on the same building blocks characterizing a general MMT, and represents a simplified base for bone tissue modeling. In particular, it assumes unidirectionally aligned mineralized fibrils. Therefore, the axial and transverse stiffness components provided by this model can be regarded as upper and lower bounds for a general MMT, where the fibrils can be arranged according to different orientation patterns [48].

We now setup and validate a new hybrid model for MTLT obtained via application of the asymptotic homogenization technique to the MCF.

### *3.2. A new hybrid multiscale model for the MTLT*

We present an alternative MTLT model by replacing the self-consistent scheme modeling the MCF in [23] with our asymptotic homogenization approach for cuboid inclusions (hybrid model (b), see Table 1). Although a comprehensive sensitivity and parametric analysis of every possible geometry and modeling assumption that could be taken into account is beyond the scope of this work, we provide this example to show how our approach can be successfully applied in a practical context. We exploit all the base values reported in [23] and focus on tissue without microporosity. The MCF is modeled as a composite made of cuboid inclusions elongated in the axial direction with an aspect ratio equal to two. Figure 6 depicts the comparison between the axial and transverse acoustic impedances obtained for the new hybrid and the Eshelby-based [23] MTLT models and how they relate to the experimental data. Note that we use, as in [23], axial and transverse acoustic impedance for this comparison because the experimental data is available in that way and it is directly related to axial and transverse stiffness, respectively; for details we refer to [23]. The relative root mean square errors (as defined

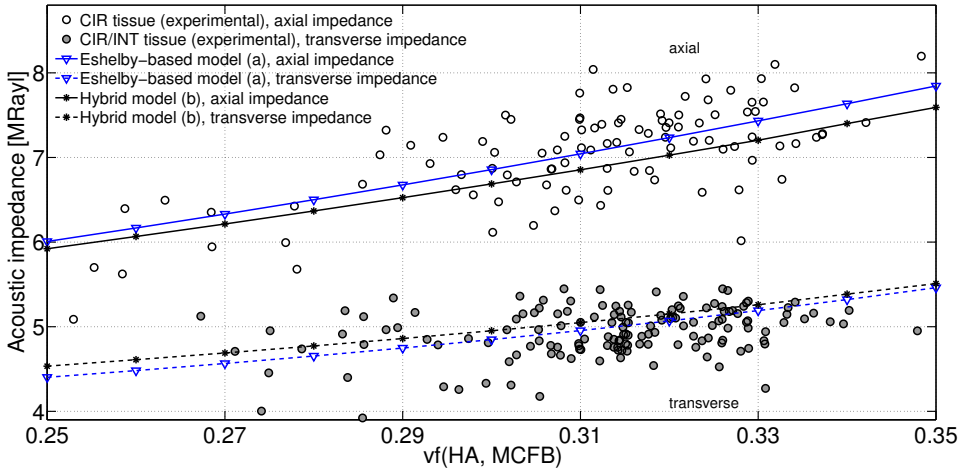


**Figure 6:** The axial and transverse acoustic impedance values obtained for the model [23] and the proposed hybrid model (b) exploiting AH in the MCF, in comparison with the experimental data (represented by circles). In both models and experimental data of circumferential (CIR) tissue, the microporosity was assumed to be negligible.

in [23]) between the Eshelby-based model [23] and the experimental data are 6.15% and 5.88% in the axial and transverse directions, respectively. The corresponding errors for the new hybrid model are 6.31% and 6.13%. Thus, a proper choice of the inclusion geometry leads to experimental validation also exploiting our asymptotic homogenization approach (here applied for the MCF).

### *3.3. A new hybrid multiscale model for MTLT with ES mineral fusion*

In this and the following section, we exploit the asymptotic homogenization approach described in Section 2 for the ES and MCF compartments within the framework of

the sequence of nested multiscale models assumed in [23] and briefly summarized in Section 3.1. The multiscale modeling of the MCFB and the MTLT tissue phases is unmodified and carried out via the Mori-Tanaka scheme. We account for the MTLT circumferential (CIR) base values reported in [23] unless otherwise specified. Every investigation presented below is performed by varying parametrically the hydroxyapatite mineral volume fraction in the MCFB, denoted by vf(HA, MCFB), in the range

$$0.25 \leq \text{vf(HA, MCFB)} \leq 0.5, \tag{13}$$

at a resolution of 1%. The mineral volume fraction is then distributed between ES and MCF according to the fraction of interfibrillar (MCF) mineral, which is assumed to be 25% in [23] according to the experimental observations reported in [49].

In this section, we assume that mineral fuses in the ES only, where the growing mineral crystals have no restrictions with respect to their structural arrangement. The self-consistent scheme, instead, is assumed to model the MCF compartment. This model is referred to as hybrid model (c), see Table 1. The ES compartment is modeled via a cross-shaped geometry and we always represent both the axial and the transverse mineral fusion areas as squares. We allow for a different relative amount of mineral fusing in the axial and transverse directions. To this end, we perform a parametric analysis by varying the ratio between the transverse and axial fusion square side lengths, denoted by $a_x = a_y$ and $a_z$, respectively, as follows

$$0.5 \leq a_x/a_z = a_y/a_z \leq 1, \tag{14}$$

for each mineral volume fraction resolved in the range given by (13). The periodic cell representing the case of equally likely mineral fusion in all three orthogonal directions, i.e. $a_x/a_z = 1$, is shown in Fig. 3, whereas the periodic cell accounting for mineral fusion where $a_x/a_z = 0.5$ is shown in Fig. 7 a).

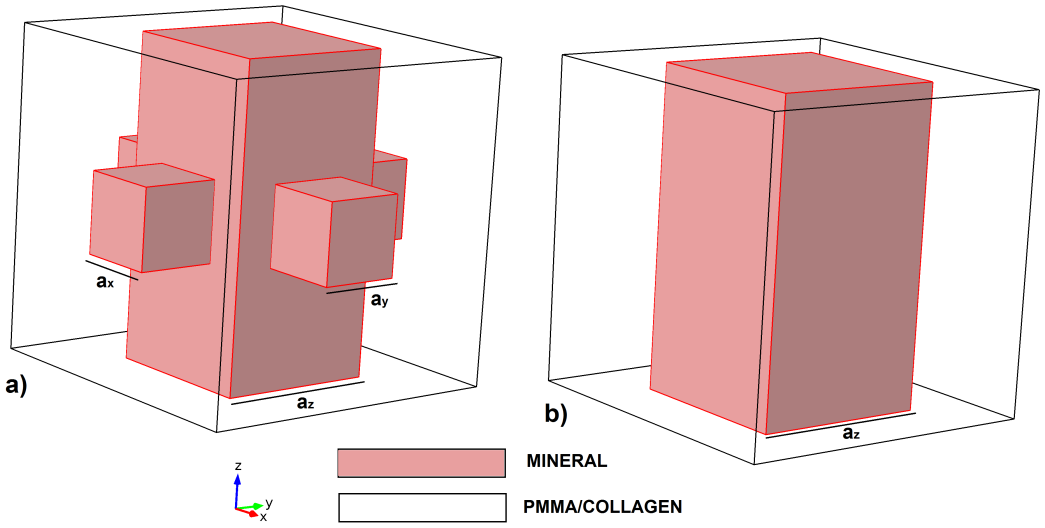


**Figure 7:** a) The periodic cell for the transverse-to-axial fusion area side ratio $a_x/a_z = 0.5$ and b) the particular case of uniaxial fusion, i.e. $a_x/a_z = 0$.

The results of this parametric study in terms of the axial ($\tilde{C}_{33}$) and transverse ($\tilde{C}_{11}$) stiffness components are shown in Fig. 8. The results from the Eshelby-based model (a) and the particular case of the hybrid model (c) with uniaxial fusing, which corresponds to $a_x/a_z = 0$, see Fig. 7 b), are also included for the sake of comparison. In the latter case, the cell problem (6-9) can be transformed into two-dimensional problems exploiting the symmetry arguments that apply for aligned fibers (see Appendix A in [31] and also [50]), further enhancing computational feasibility of the AH approach. In addition, in Fig. 8 a), we also show the full data from the interstitial human radius axial stiffness [25], including those not falling within the range given by mean ± standard deviation as identified in [25].

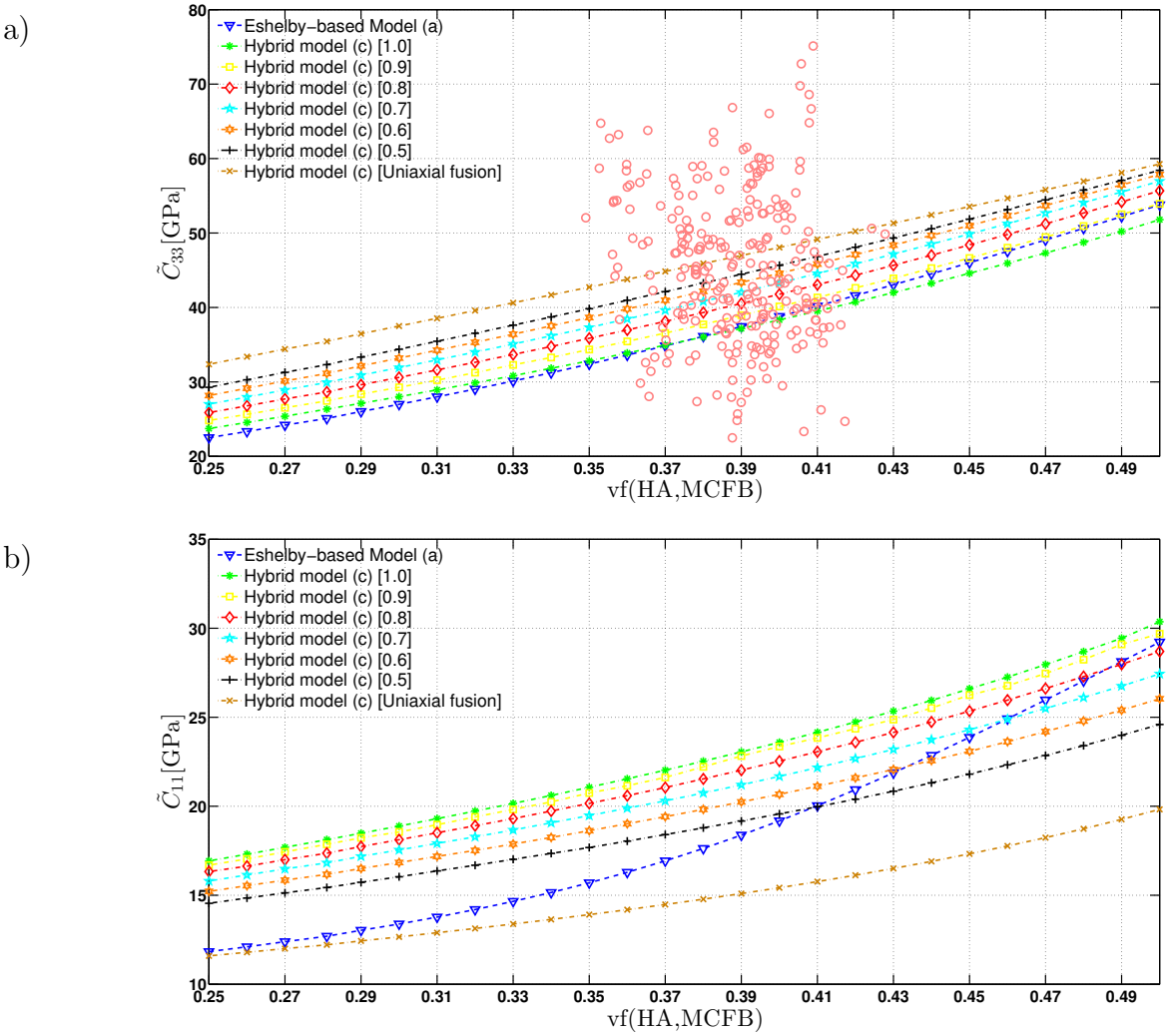


**Figure 8:** The axial stiffness $\tilde{C}_{33}$ (top plot) and the transverse stiffness $\tilde{C}_{11}$ (bottom plot) as functions of the mineral volume fraction. For the hybrid model (c), the ratio $a_x/a_z$ for fusing in the ES is given in square brackets. The human radius axial stiffness data from [25] are represented as circles in a).

Mineral fusing has a relevant quantitative impact on the elasticity tensor components, even when occurring in the ES only. The axial stiffness $\tilde{C}_{33}$ is characterized by an $\approx 30\%$ increase (with respect to the MTLT model [23]), when moving towards

the limit case (i.e. axial fusing only) for $0.37 < \text{vf(HA, MCFB)} < 0.40$, that is the mineral volume fraction range that pertains to most of the experimental data according to the statistical analysis reported in [25]. The stiffness in the transverse direction ($\tilde{C}_{11}$), instead, reaches its maximum value when the fusing is equally-likely occurring in each orthogonal direction ($a_x/a_z = 1$). In general, both the axial and the transverse stiffness components increase, compared to the Eshelby-based model (a) and in that range of mineral volume fraction, in the explored range of $a_x/a_z$ (the transverse component only is found to be lower than the MTLT model [23] in the limit case of uniaxial fusing).

### *3.4. A new hybrid multiscale model for MTLT with ES and MCF mineral fusion*

We conclude the section quantifying the effect of mineral fusing also in the MCF compartment via our hybrid asymptotic homogenization/Eshelby-based approach for cross-shaped structures. Since, according to [49], only 25% of the global mineral content is present in the MCF, the elastic stiffness components are primarily influenced by variations in the ES compartment. However, we aim at determining the maximum axial stiffening that can be captured by our model and observe to what extent the experimental results [25] fall within the range we provide. To this end, we focus on uniaxial fusing in the ES compartment, and perform a parametric analysis by varying the ratio $a_x/a_z$ in the MCF (hybrid model (d), cf. Table 1). The results for $\tilde{C}_{33}$ and $\tilde{C}_{11}$ are shown in Fig. 9. The axial stiffness exhibits the same monotonically and linearly increasing (with respect to the mineral volume fraction) profile that characterizes mineral fusing in the ES compartment only. However, we obtain a further increase of the elastic stiffness. The particular case of uniaxial fusing in both compartments represents an upper bound for the axial stiffness. This particular case also represents a lower bound for the transverse stiffness, as in this case the mineral phase corresponds, in both compartments, to reinforcing fibers aligned along the axial direction.

The results in this section, compared to those shown in [23], see also Fig. 2, show a remarkably better agreement with the experimental axial stiffness in the aged interstitial human radius data from [25].

## 4. Discussion

In this paper we have combined the potential of the asymptotic homogenization approach [31, 32] with the MTLT hierarchical model [23] to setup an innovative multiscale framework for musculoskeletal mineralized tissues. The major novelty resides in incorporating and quantifying the effect of mineral fusing reported for mature bone [27]. This effect can explain the remarkably high axial stiffness values of aged cortical bone that do not fall within the bounds reported in [23].

We have started depicting the main features of the asymptotic homogenization technique for elastic composites with discontinuous materials properties in Section 2. In Section 2.1 we have performed a three-dimensional test to compute the elastic stiffness

a)

b)

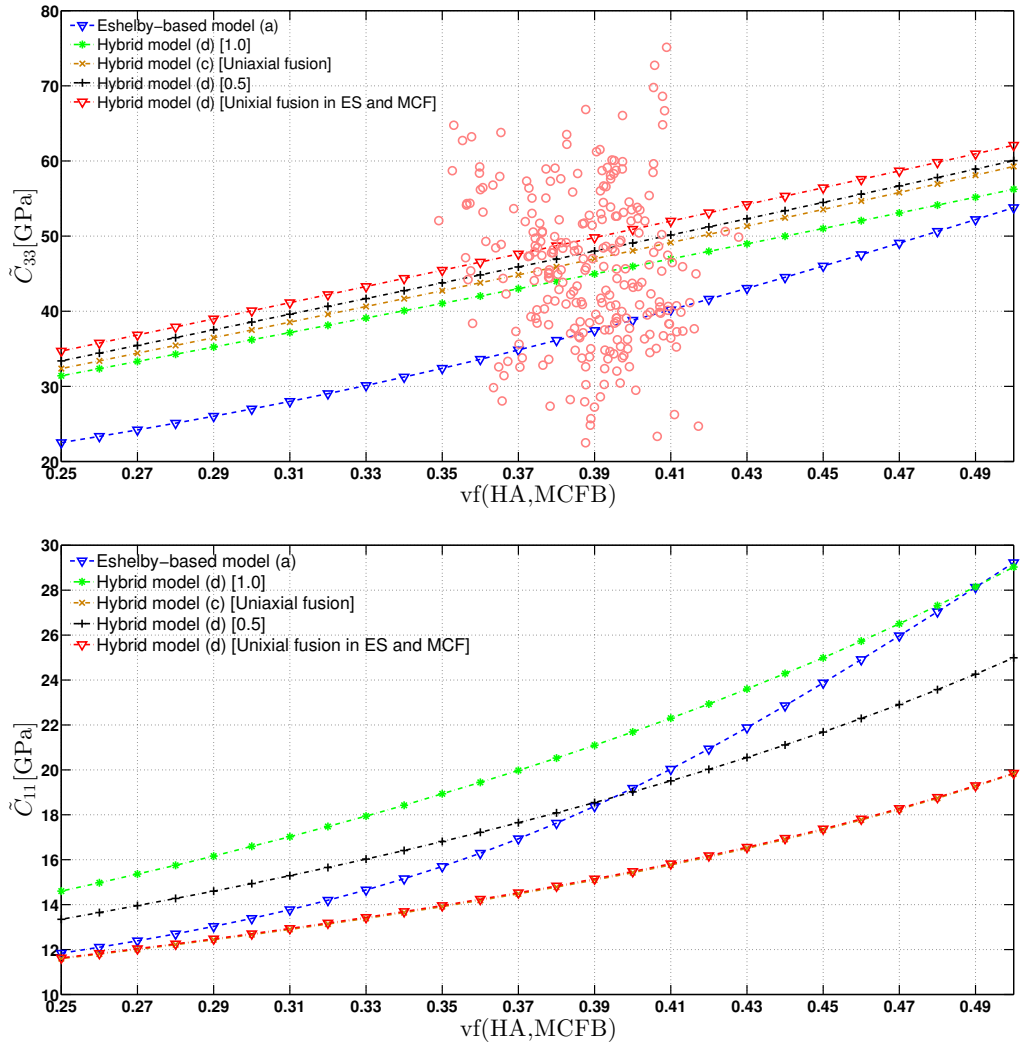


**Figure 9:** The axial stiffness $\tilde{C}_{33}$ (top plot) and the transverse stiffness $\tilde{C}_{11}$ (bottom plot) as functions of the mineral volume fraction. For the hybrid model (d), the ratio $a_x/a_z$ for fusing in the MCF is given in square brackets and uniaxial fusing in the ES is used. The human radius axial stiffness data from [25] are represented as circles in a).

of a fused structure surrounded by a softer matrix. Our results, when compared to those obtained for single cubic inclusions, show a significant stiffening solely due to the cross-shaped structure, which represents the fused material in a periodic setting. This example may be of crucial importance to support an informed design of artificial/biomimetic elastic materials, when it is required to increase the overall composite stiffness without further increasing the volume fraction of the embedded stiffer phase.

In Section 3 we have implemented several hybrid Eshelby-based/asymptotic homogenization hierarchical model based on the MTLT model [23] that is capable to describe mineralized tissues to different extents. After summarizing the main features of [23] in Section 3.1, we have presented a hybrid hierarchical approach by modeling the MCF via asymptotic homogenization, representing the mineral as cuboid inclusions. Our results compare well with the MTLT experimental data reported in [23] and demonstrate

that the AH technique is reliable when used in the context of this practical application. The validation shown by Fig. 6 is not surprising, as, by replacing the self-consistent scheme with asymptotic homogenization in the MCF, we still fully retain the interactions between phases, as highlighted in [31]. Furthermore, we note that in our simulations, replacing the self-consistent scheme by the asymptotic homogenization approach does not affect the overall computing time which remains in the order of minutes. Although in the latter approach three-dimensional finite element calculations are involved, the former scheme requires an almost equally expensive solution of a highly nonlinear system of equations.

In Section 3.2 we apply our asymptotic homogenization scheme to the ES performing a parametric analysis to investigate variations of the transverse and axial stiffness at increasing amount of mineral fusing in the axial direction (ranging from equally-likely to uniaxial fusing), for a wide range of physiological mineral volume fractions (up to 50%). In Section 3.3, we perform the same analysis in the MCF assuming uniaxial fusing in the ES (where most of the mineral content resides), reaching the highest possible axial stiffness that can be captured via our hybrid modeling approach.

The transverse stiffness is inversely correlated with the amount of mineral fusing in the axial direction and the highest transverse stiffness profile is observed for equally-likely fusing in the ES only, see Fig. 8 b), Hybrid model (c) [1.0]. The self-consistent scheme used in [23] considers ellipsoidal inclusions highly elongated in the axial directions, thus explaining the higher transverse stiffness values observed for non-uniaxial mineral fusing in ES only, up to 40% mineral volume fraction. However, the stiffness vs. mineral volume fraction profile for the self-consistent scheme is nonlinearly increasing and the stiffness values become comparable to those for equally likely fusion when the 50% mineral volume fraction upper limit is reached.

Axial stiffness is, instead, directly correlated with the mineral fusing in the axial direction. In this case, an increasing amount of mineral fusing in the axial direction leads to stiffness values significantly higher than those of [23], see Figs. 8 a) and 9 a). Our parametric analysis shows that also the fusing mechanism, together with the increase of the mineral volume fraction, drives stiffening for mineralized tissues. We have compared our results to the aged bone data that fall outside the bounds provided in [23], focusing on the interstitial human radius [25], which exhibits the highest (detectable) axial stiffness values ([23], Table 3, page 1019). According to the mean and standard deviation values reported in [25] and taking ranges as mean $\pm$ standard deviation, most of the experimental axial stiffness values are in the range from 35.5 to 55.7 GPa and most of the experimental mineral volume fraction values are in the range from 37 to 40 %. In the latter volume fractions range, we report axial stiffness values from 35 GPa (Hybrid model (c) [1.0]) to 50.4 GPa (Hybrid model (d) [Uniaxial fusion in ES and MCF]). We thus obtain a good agreement with the considered experimental data for aged human radius. Our analysis clearly shows that the increase in axial stiffness is not only influenced by the amount of mineral, but also by the presence of mineral fusing in different directions. The latter can play a crucial role in determining the stiffening of the whole MMT.

The distribution of the experimental data points is apparently counterintuitive, as their axial stiffness values are not always monotonically increasing with the mineral volume fraction. According to our analysis, these results can be simply explained accounting for the fusion mechanism, which can occur to a different extent in the axial/transverse directions and/or in the MCF/ES compartments.

## 5. Conclusions

The novel modeling approach we have presented here involves several simplifying assumptions and is open to improvements. In this paper, as well as in [23], we have considered a stationary, linear elastic modeling approach for every hierarchical level considered in the sequence of nested models. We have neglected (a) the different mineralization mechanisms occurring inter- and extrafibrillarly via growth of the mineral crystals, which are related to the formation of the interconnections leading to the formation of a continuous mineral foam, (b) the interplay between water and the various MMT constituents, (c) a potential aging-related effect on the collagen volume fraction, (d) the plastic nature of the bone tissue and any aging-related issue concerning changes of strength and toughness.

Hydroxyapatite crystals nucleate within the gap region between adjacent collagen fibrils and align along the bone axis during maturation of long bones [51]. Extrafibrillar mineralization, as reported in [52, 53], occurs via appositional coating around the collagen fibrils, as considered in the micromechanical model [54]. We have chosen our cross-shaped structures as a proxy that resembles the fused mineralized skeleton that is experimentally observed in mature bone [28]. Although we believe that this approximation is well-grounded as a first step, future modeling approaches should carefully consider the difference between the mineral fusing processes taking place in the MCF and the ES and how they interplay with mineral growth, as this may lead to consider different geometries (depending on the growth stage), that can in turn modify the resulting MMT stiffness. Although the process of mineral nucleation into the organic matrix is not yet fully understood, possible mechanisms are identified in the precipitation of calcium phosphate solutions or calcium binding protein molecules interactions. This implies, in turn, a crucial interplay with water, especially, but not solely, on the nanoscale, as highlighted in [55].

Water is actually one of the major constituents of MMTs [5], and almost every hierarchical level can be considered as a poroelastic material [56]. In this paper we have dealt with a simplified scenario, representing the nanopores as a linear elastic material (pmma), as in [23], where this choice is dictated by the actual experimental setting at hand. A more accurate description of the ES should account for the fluid structure interaction between the slowly-flowing water (containing calcium ions) and mineral crystals, and address the complex issue of appositional growth via a mass exchange between the fluid (water) and solid (mineral) phase to reach an effective representation of the compound as a poroelastic growing material [57].

As a first approximation, we have neglected the microporosity contribution (thus using the 0% base value reported in [23] for circumferential MTLT tissue, where the microporosity is likewise approximated as an elastic material), as water content has been proven to be inversely proportional to the mineral content [58] (and, as a consequence, to elastic stiffness), where the latter is supposed to increase during hypermineralization. The qualitative stiffening profile deduced by the present analysis is actually not affected by changes in microporosity within the range reported in [23] (0-10%), whereas the quantitative results regarding axial stiffening amount to a decrease of up to 10% for 10% microporosity. However, the role of water should be carefully addressed in future works, depending on the particular bone tissue and hierarchical level under investigation. This constituent can not only influence the overall MMT stiffness, but can also affect other important mechanical properties such as toughness.

In our present MMT model, we compute, as detailed in [23], the collagen volume fraction from the prescribed mineral volume fraction using the empirical formula as documented in [25]. That empirical relationship, while validated against diverse experimental data, might, however, have to be adapted for aged bone tissue. To the best of the authors knowledge this issue has not been discussed yet in the literature. If there were an influence on the collagen volume fraction with tissue aging, this would then also contribute to partially explain the variation of the experimental elastic stiffness detected for the same mineral volume fraction, cf. Figure 2. This effect would then add to or interact with the effect that mineral fusion has on the stiffness for fixed mineral volume fraction as discussed in this study.

The toughness, which is not considered in this work, is related to the resistance to fracture, and this is dramatically affected by aging [59]. Recent studies have demonstrated that MMTs become more brittle as a consequence of collagen cross-links reduction [60]. Experimental evidence of toughness reduction via heat-induced collagen denaturation has been reported in [8]. Careful investigation of these mechanical aspects cannot be carried out via a linear elastic framework, and a future challenge resides in an appropriate plastic constitutive relationship for the collagen behavior in a multiscale modeling framework, as highlighted in [61].

Our modeling framework represents a first, fundamental step towards the multiscale modeling of aging effects in bone tissue. We are able to show that the stiffening of aged bone is actually related to the constitution of a continuous mineral foam. This modeling framework at hand can provide unique insights towards an efficient design of biomimetic materials making use of continuous and interconnected stiffening structures.

However, a number of intriguing challenges remain to be addressed towards a comprehensive hierarchical model of musculoskeletal mineralized tissues that can fully include the mechanical and chemical role of the various constituents and their interplay with age related modifications.

**Acknowledgements**

This work was supported by the DFG priority program SPP 1420, project GE 1894/3 and RA 1380/7 *Multiscale structure-functional modeling of musculoskeletal mineralized tissues*, PIs Alf Gerisch and Kay Raum. The authors would like to sincerely thank Eli Duenisch for programming support and Sara Tiburtius for insightful discussions about the content of this work.

## References

[1] Derek Hull and TW Clyne. *An introduction to composite materials*. Cambridge university press, 1996.

[2] Andrej Cherkaev and Robert Kohn. *Topics in the mathematical modelling of composite materials*. Springer, 1997.

[3] Robert M Jones. *Mechanics of composite materials*. CRC Press, 1998.

[4] Graeme W Milton. *The theory of composites*, volume 6. Cambridge University Press, 2002.

[5] S. Weiner and H. D. Wagner. The material bone: Structure-mechanical function relations. *Annual Reviews of Materials Science*, 28:271–298, 1998.

[6] Peter Fratzl and Richard Weinkamer. Natures hierarchical materials. *Progress in Materials Science*, 52(8):1263–1334, 2007.

[7] E Hamed, E Novitskaya, J Li, P-Y Chen, I Jasiuk, and J McKittrick. Elastic moduli of untreated, demineralized and deproteinized cortical bone: validation of a theoretical model of bone as an interpenetrating composite material. *Acta biomaterialia*, 8(3):1080–1092, 2012.

[8] Xiaodu Wang, Ruud A Bank, Johan M TeKoppele, and C Agrawal. The role of collagen in determining bone mechanical properties. *Journal of orthopaedic research*, 19(6):1021–1026, 2001.

[9] John D Currey. The relationship between the stiffness and the mineral content of bone. *Journal of biomechanics*, 2(4):477–480, 1969.

[10] HL Cox. The elasticity and strength of paper and other fibrous materials. *British journal of applied physics*, 3(3):72, 1952.

[11] H Daniel Wagner and Steve Weiner. On the relationship between the microstructure of bone and its mechanical stiffness. *Journal of Biomechanics*, 25(11):1311–1320, 1992.

[12] JE Ashton, JC Halpin, and PH Petit. Primer on composite analysis. *Technomic, Stamford, CN*, 1969.

[13] Ingomar Jäger and Peter Fratzl. Mineralized collagen fibrils: a mechanical model with a staggered arrangement of mineral particles. *Biophysical Journal*, 79(4):1737–1746, 2000.

[14] J.D. Eshelby. The determination of the elastic field of an ellipsoidal inclusion, and related problems. *Proceedings of the Royal Society of London. Series A. Mathematical and Physical Sciences*, 241:376–396, 1957.

[15] Christian Hellmich and Franz-Josef Ulm. Micromechanical model for ultrastructural stiffness of mineralized tissues. *Journal of Engineering Mechanics*, 128(8):898–908, 2002.

[16] Christian Hellmich, Jean-Francois Barthélémy, and Luc Dormieux. Mineral–collagen interactions in elasticity of bone ultrastructure–a continuum micromechanics approach. *European Journal of Mechanics-A/Solids*, 23(5):783–810, 2004.

[17] Ozan Akkus. Elastic deformation of mineralized collagen fibrils: an equivalent inclusion based composite model. *Journal of biomechanical engineering*, 127(3):383–390, 2005.

[18] Young June Yoon and Stephen C. Cowin. The estimated elastic constants for a single bone osteonal lamella. *Biomechanics and Modeling in Mechanobiology*, 7(1):1–11, 2007.

[19] Andreas G Reisinger, Dieter H Pahr, and Philippe K Zysset. Sensitivity analysis and parametric

study of elastic properties of an unidirectional mineralized bone fibril-array using mean field methods. *Biomechanics and modeling in mechanobiology*, 9(5):499–510, 2010.

[20] Quentin Grimal, Guillermo Rus, William J Parnell, and Pascal Laugier. A two-parameter model of the effective elastic tensor for cortical bone. *Journal of biomechanics*, 44(8):1621–1625, 2011.

[21] Claire Morin and Christian Hellmich. A multiscale poromicromechanical approach to wave propagation and attenuation in bone. *Ultrasonics*, 54(5):1251–1269, 2014.

[22] André Zaoui. Continuum micromechanics: Survey. *Journal of Engineering Mechanics*, 128(8):808–816, 2002.

[23] Sara Tiburtius, Susanne Schrof, Ferenc Molnár, Peter Varga, Françoise Peyrin, Quentin Grimal, Kay Raum, and Alf Gerisch. On the elastic properties of mineralized turkey leg tendon tissue: multiscale model and experiment. *Biomechanics and modeling in mechanobiology*, 13:1003–1023, 2014.

[24] Daniel Rohrbach, Sannachi Lakshmanan, Françoise Peyrin, Max Langer, Alf Gerisch, Quentin Grimal, Pascal Laugier, and Kay Raum. Spatial distribution of tissue level properties in a human femoral cortical bone. *Journal of biomechanics*, 45(13):2264–2270, 2012.

[25] K. Raum, R. O. Cleveland, F. Peyrin, and P. Laugier. Derivation of elastic stiffness from site-matched mineral density and acoustic impedance maps. *Physics in Medicine and Biology*, 51(3):747–758, 2006.

[26] Kay Raum, Tobias Hofmann, Ingrid Leguerney, Amena Saïed, Françoise Peyrin, Laurence Vico, and Pascal Laugier. Variations of microstructure, mineral density and tissue elasticity in b6/c3h mice. *Bone*, 41(6):1017–1024, 2007.

[27] Po-Yu Chen, Damon Toroian, Paul A Price, and Joanna McKittrick. Minerals form a continuum phase in mature cancellous bone. *Calcified tissue international*, 88(5):351–361, 2011.

[28] V Benezra Rosen, LW Hobbs, and M Spector. The ultrastructure of anorganic bovine bone and selected synthetic hyroxyapatites used as bone graft substitute materials. *Biomaterials*, 23(3):921–928, 2002.

[29] Erika Davies, Karin H Müller, Wai Ching Wong, Chris J Pickard, David G Reid, Jeremy N Skepper, and Melinda J Duer. Citrate bridges between mineral platelets in bone. *Proceedings of the National Academy of Sciences*, 111(14):E1354–E1363, 2014.

[30] Petar Milovanovic, Jelena Potocnik, Danijela Djonic, Slobodan Nikolic, Vladimir Zivkovic, Marija Djuric, and Zlatko Rakocevic. Age-related deterioration in trabecular bone mechanical properties at material level: nanoindentation study of the femoral neck in women by using afm. *Experimental gerontology*, 47(2):154–159, 2012.

[31] R Penta and Alf Gerisch. Investigation of the potential of asymptotic homogenization for elastic composites via a three-dimensional computational study. *Computing and Visualization in Science*, doi: 10.1007/s00791-015-0257-8(-):1–17, 2016.

[32] R Penta and Alf Gerisch. The asymptotic hmoogenization elasticity tensor properties for composites with material discontinuities. *Ccontinuum Mechanics and Thermodynamics*, -(Submitted):1–25, 2015.

[33] G Papanicolau, A Bensoussan, and J-L Lions. *Asymptotic analysis for periodic structures*. Elsevier, 1978.

[34] E. Sanchez-Palencia. *Non-Homogeneous Media and Vibration Theory-Lecture Notes in Physics 127*. Springer-Verlag, 1980.

[35] Nikolaï Bakhvalov and G Panasenko. *Homogenisation averaging processes in periodic media*. Springer, 1989.

[36] Grégoire Allaire. Homogenization and two-scale convergence. *SIAM Journal on Mathematical Analysis*, 23(6):1482–1518, 1992.

[37] M. Holmes. *Introduction to perturbation method*. Springer-Verlag, 1995.

[38] Jean-Louis Auriault, Claude Boutin, and Christian Geindreau. *Homogenization of coupled phenomena in heterogenous media*, volume 149. John Wiley & Sons, 2010.

[39] C. C. Mei and B. Vernescu. *Homogenization Methods for multiscale mechanics*. World Scientific,

2010.

[40] Michael A Slawinski. *Waves and rays in elastic continua*. World Scientific, 2010.

[41] Andrei Constantinescu and Alexander Korsunsky. *Elasticity with Mathematica: An Introduction to Continuum Mechanics and Linear Elasticity*. Cambridge University Press, 2007.

[42] JMJ Den Toonder, JAW Van Dommelen, and FPT Baaijens. The relation between single crystal elasticity and the effective elastic behaviour of polycrystalline materials: theory, measurement and computation. *Modelling and Simulation in Materials Science and Engineering*, 7(6):909, 1999.

[43] Benjamin Alexander, Tyrone L Daulton, Guy M Genin, Justin Lipner, Jill D Pasteris, Brigitte Wopenka, and Stavros Thomopoulos. The nanometre-scale physiology of bone: steric modelling and scanning transmission electron microscopy of collagen–mineral structure. *Journal of the Royal Society Interface*, page rsif20110880, 2012.

[44] W. Voigt. Ueber die Beziehung zwischen den beiden Elasticitätsconstanten isotroper Körper. *Annalen der Physik und Chemie, Neue Folge*, 38:573–587, 1888.

[45] A. Reuss. Berechnung der Fließgrenze von Mischkristallen auf Grund der Plastizitätsbedingung für Einkristalle. *ZAMM - Journal of Applied Mathematics and Mechanics / Zeitschrift fr Angewandte Mathematik und Mechanik*, 9(1):49–58, 1929.

[46] R. Hill. A self-consistent mechanics of composite materials. *Journal of the Mechanics and Physics of Solids*, 13(4):213–222, 1965.

[47] T. Mori and K. Tanaka. Average stress in matrix and average elastic energy of materials with misfitting inclusions. *Acta Metallurgica*, 21(5):571–574, 1973.

[48] Peter Varga, Alexandra Pacureanu, Max Langer, Heikki Suhonen, Bernhard Hesse, Quentin Grimal, Peter Cloetens, Kay Raum, and Françoise Peyrin. Investigation of the three-dimensional orientation of mineralized collagen fibrils in human lamellar bone using synchrotron x-ray phase nano-tomography. *Acta biomaterialia*, 9(9):8118–8127, 2013.

[49] S. Lees, K. S. Prostak, V. K. Ingle, and K. Kjoller. The loci of mineral in turkey leg tendon as seen by atomic force microscope and electron microscopy. *Calcified Tissue International*, 55(3):180–189, 1994.

[50] W J Parnell and I D Abrahams. Homogenization for wave propagation in periodic fibre-reinforced media with complex microstructure. I. Theory. *Journal of the Mechanics and Physics of Solids*, 56(7):2521–2540, 2008.

[51] Peter Fratzl, Nadja Fratzl-Zelman, Klaus Klaushofer, Gero Vogl, and Kristian Koller. Nucleation and growth of mineral crystals in bone studied by small-angle x-ray scattering. *Calcified tissue international*, 48(6):407–413, 1991.

[52] Tue Hassenkam, Georg E Fantner, Jacqueline A Cutroni, James C Weaver, Daniel E Morse, and Paul K Hansma. High-resolution afm imaging of intact and fractured trabecular bone. *Bone*, 35(1):4–10, 2004.

[53] JH Kindt, PJ Thurner, ME Lauer, BL Bosma, Georg Schitter, Georg E Fantner, Michi Izumi, James C Weaver, Daniel E Morse, and Paul K Hansma. In situ observation of fluoride-ion-induced hydroxyapatite–collagen detachment on bone fracture surfaces by atomic force microscopy. *Nanotechnology*, 18(13):135102, 2007.

[54] Svetoslav Nikolov and Dierk Raabe. Hierarchical modeling of the elastic properties of bone at submicron scales: the role of extrafibrillar mineralization. *Biophysical journal*, 94(11):4220–4232, 2008.

[55] Erin E Wilson, Ayorinde Awonusi, Michael D Morris, David H Kohn, Mary MJ Tecklenburg, and Larry W Beck. Three structural roles for water in bone observed by solid-state nmr. *Biophysical journal*, 90(10):3722–3731, 2006.

[56] Stephen C Cowin. Bone poroelasticity. *Journal of biomechanics*, 32(3):217–238, 1999.

[57] R. Penta, D. Ambrosi, and R. J. Shipley. Effective governing equations for poroelastic growing media. *The Quarterly Journal of Mechanics and Applied Mathematics*, 67(1):69–91, 2014.

[58] Maria A Fernández-Seara, Suzanne L Wehrli, Masaya Takahashi, and Felix W Wehrli. Water

content measured by proton-deuteron exchange nmr predicts bone mineral density and mechanical properties. *Journal of Bone and Mineral Research*, 19(2):289–296, 2004.

[59] M Grynpas. Age and disease-related changes in the mineral of bone. *Calcified tissue international*, 53(1):S57–S64, 1993.

[60] H Oxlund, M Barckman, G Ørtoft, and TT Andreassen. Reduced concentrations of collagen cross-links are associated with reduced strength of bone. *Bone*, 17(4):S365–S371, 1995.

[61] Robert O Ritchie, Markus J Buehler, and Paul Hansma. Plasticity and toughness in bone. *Phys Today*, 62(6):41–47, 2009.